Implementation of a Hybrid DFT Method for Calculating NMR Shieldings Using Slater-Type Orbitals with Spin−Orbital Coupling Included. Applications to ^{187}Os, ^{195}Pt, and ^{13}C in Heavy-Metal Complexes†

Mykhaylo Krykunov,‡ Tom Ziegler,*,‡ and Erik van Lenthe§

Department of Chemistry, University of Calgary, Calgary T2N 1N4, Alberta, Canada, and Afdeling Theoretische Chemie, Vrije Universiteit, De Boelelaan 1083, 1081 HV Amsterdam, The Netherlands

Received: March 4, 2009; Revised Manuscript Received: July 28, 2009

We report on the implementation of an algorithm for the calculation of the NMR shielding tensor. Our scheme is based on the Hartree−Fock method and the zeroth-order regular approximation (ZORA) Hamiltonian with spin−orbital coupling included. Gauge-including atomic orbitals (GIAOs) are employed to ensure the origin invariance of the results. Unlike the previous implementation by Fukui and Baba [*J. Chem. Phys.* **2002**, *117*, 7836], our computational scheme makes use of Slater-type orbitals. We have employed this method in B3LYP calculations of the ^{13}C, ^{195}Pt, and ^{187}Os NMR chemical shifts in 5d metal carbonyls, Pt(II) square-planar complexes, and osmium phosphines, respectively. The calculated NMR chemical shifts are compared to the results obtained with the BP86 and BLYP functionals, as well as the Hartree−Fock method. Comparisons are also given to experimental values. For the ^{195}Pt chemical shifts, we have found a small improvement with respect to experiment for the B3LYP results over the BP86 and BLYP values. For the other systems, use of the B3LYP method does not improve the agreement with experiment compared to results from pure functionals such as BP86 and BLYP.

1. Introduction

A theoretical description of the NMR chemical shifts of heavy elements requires taking into account relativistic effects.[1] For large molecules, a combination of the two-component ZORA method along with DFT affords reasonably accurate NMR chemical shifts at a relatively small computational cost. Such a computational scheme has been implemented by Wolff et al.[2] for pure functionals. However, this implementation makes use of Slater-type orbitals (STOs), and it was, as a result, not at that time possible to extend the scheme to hybrid density functionals. Fukui and Baba[3] have implemented the ZORA method for the Gaussian-type orbitals (GTOs) at the Hartree−Fock level of theory. By making use of a recently developed double fitting algorithm for the calculation of the Hartree−Fock exchange integrals with STOs,[4] it has now become possible to apply the scalar ZORA method in conjunction with hybrid functionals to the calculation of the NMR shielding tensor using STOs. Other applications of the double fitting algorithm for the calculation of the exact Hartree−Fock exchange with STOs include the implementation of the spin−spin coupling constants,[5] the static and dynamic second hyperpolarizability,[6] and the exact exchange optimized effective potential method.[7]

The aim of this work is a further extension of our ZORA hybrid functional scheme for the calculation of the NMR shielding tensor to the case where spin−orbital coupling is included. We have tested our implementation on the ^{13}C chemical shifts in 5d metal carbonyls and ^{195}Pt chemical shifts in Pt(II) square-planar complexes. These systems were previously studied with nonhybrid functionals,[8,9] and it was shown that the spin−orbital coupling is important for an accurate description of the NMR chemical shifts. In both cases, experimental trends were reflected in the calculated chemical shifts. However, obtaining good agreement with experiment for square platinum complexes is a very difficult task, unlike the case of Pt(IV) species for which excellent agreement between theory and experiment has been reported.[10−12] Since ^{195}Pt shifts are measured in solutions, Sterzel and Autschbach[13] have argued that for an accurate theoretical description of the Pt NMR chemical shifts, solvation effects have to be taken into account with explicit consideration of solvation shells. The results of theoretical modeling of the ^{195}Pt NMR shifts have been reviewed in refs 14−16.

We have, in addition, applied the hybrid DFT/ZORA computation scheme to the calculation of the ^{187}Os NMR chemical shifts in osmium complexes. These systems have not been studied computationally before.

Apart from transition-metal complexes, it was also decided to test our implementation on the proton NMR chemical shifts in hydrogen halides because they have been studied at the two-component ZORA/Hartree−Fock level of theory[3] as well as by other relativistic theoretical methods.[8,17,18]

In the next section, we shall briefly outline the computational scheme, which incorporates the double fitting technique for the calculation of the Hartree−Fock exchange integrals. In section 3, we give the computational details. In section 4, we present the results of the calculations and discuss the results. The conclusions are outlined in section 5.

2. Implementation Details

The calculation of the NMR shielding tensor as a second-order derivative of the total electronic energy expression requires the knowledge of the first-order perturbed Kohn−Sham orbitals. As was previously shown,[2] the NMR shielding tensor for the

† Part of the "Walter Thiel Festschrift".

* To whom correspondence should be addressed. E-mail: ziegler@ucalgary.ca. Fax: (403)289-9488. Phone: (403)220-5368.

‡ University of Calgary.

§ Vrije Universiteit.

10.1021/jp901991s CCC: $40.75
Published on Web 09/04/2009

ZORA Hamiltonian with spin−orbital coupling can be written as a sum of three contributions in terms of the paramagnetic, the diamagnetic, and the spin−orbit part. Similar to refs 2 and 3, we make use in this work of the ZORA Hamiltonian perturbed by a magnetic field

$$F^{\mathrm{ZORA}} = \boldsymbol{\sigma}\cdot\left(\mathbf{p} + \frac{1}{c}\mathbf{A}_{\mathrm{B}}\right)\frac{c^2}{2c^2 - V}\boldsymbol{\sigma}\cdot\left(\mathbf{p} + \frac{1}{c}\mathbf{A}_{\mathrm{B}}\right) + V - aK \tag{1}$$

for the calculation of the first-order perturbed Kohn−Sham orbitals

$$\psi_i^{\gamma,(1)}(\mathbf{B}) = \sum_j^{\mathrm{all}} u_{ji}^{(1)}\psi_j^{\gamma,(0)} = \sum_j^{\mathrm{all}}\sum_\mu u_{ji}^{(1)} d_{\mu j}^{\gamma}\chi_\mu \tag{2}$$

where ψ_i^{γ} is the two-component ZORA orbital, γ - the spin function (α or β), χ_μ is an atomic basis function, $d_{\mu j}^{\gamma}$ is the expansion coefficient of the unperturbed orbital, $\boldsymbol{\sigma}$ is the Pauli spin matrices, $\mathbf{p}$ is the momentum operator, c is the velocity of light, $\mathbf{A}_{\mathrm{B}}$ is the magnetic vector potential, K is the exchange operator, and a is the admixture coefficient of the exact Hartree−Fock exchange. The potential V includes the nuclear attraction potential, the electrostatic Coulomb potential, and a local part of the Kohn−Sham potential

$$V = V_{\mathrm{nuc}} + V_{\mathrm{C}} + (1 - a)V_{\mathrm{XC}} \tag{3}$$

The $u^{(1)}$ matrices are obtained from the first-order perturbation theory

$$u_{ki,t}^{(1)} = -\frac{1}{2}S_{ki,t}^{(1)} \qquad (i,k \in \mathrm{occ}) \tag{4}$$

$$u_{ai,t}^{(1)} = \frac{F_{ai,t}^{(1)} - \varepsilon_i^0 S_{ai,t}^{(1)}}{\varepsilon_i^0 - \varepsilon_a^0} \qquad (i \in \mathrm{occ}\ \mathrm{and}\ a \in \mathrm{virt}) \tag{5}$$

Here, t is a Cartesian component of the magnetic perturbation, ε_k^0 are scaled ZORA orbital energies[19]

$$F_{ai,t}^{(1)} = \sum_{\mu,\nu}\sum_{\gamma,\gamma'} d_{\mu a}^{\gamma *} F_{\mu\nu,t}^{\gamma\gamma',(1)} d_{\nu i}^{\gamma'} \tag{6}$$

and

$$S_{ji,t}^{(1)} = \sum_{\mu,\nu}\sum_{\gamma,\gamma'} d_{\mu j}^{\gamma *} S_{\mu\nu,t}^{\gamma\gamma',(1)} d_{\nu i}^{\gamma'} \tag{7}$$

with

$$S_{\mu\nu,t}^{\gamma\gamma',(1)} = \frac{\mathrm{i}}{2c}\langle\chi_\mu\gamma|[\mathbf{r}\times(\mathbf{R}_\nu - \mathbf{R}_\mu)]_t|\chi_\nu\gamma'\rangle \tag{8}$$

$$\begin{aligned} F_{\mu\nu,t}^{\gamma\gamma',(1)} = {} & \langle\chi_\mu|\frac{K}{4c}[\mathbf{r}_\mu\times\mathbf{p}]_t + \frac{K}{4c}[\mathbf{r}_\nu\times\mathbf{p}]_t|\chi_\nu\rangle + \\ & \langle\chi_\mu|\frac{\mathrm{i}V}{2c}[\mathbf{r}\times(\mathbf{R}_\nu - \mathbf{R}_\mu)]_t + \mathbf{p}\cdot\frac{\mathrm{i}K}{4c}[\mathbf{r}\times(\mathbf{R}_\nu - \mathbf{R}_\mu)]_t\mathbf{p}|\chi_\nu\rangle + \\ & \langle\chi_\mu\gamma|\boldsymbol{\sigma}\cdot\left[\nabla\left(\mathrm{i}\frac{K-1}{4c}[\mathbf{r}\times(\mathbf{R}_\nu - \mathbf{R}_\mu)]_t\right)\times\mathbf{p}\right]|\chi_\nu\gamma'\rangle + \\ & \langle\chi_\mu\gamma|\frac{1}{2c}\boldsymbol{\sigma}_t - \mathrm{i}\frac{K-1}{4c}\boldsymbol{\sigma}_t\mathbf{r}_\mu\cdot\mathbf{p} + \mathbf{p}\cdot\mathbf{r}_\nu\boldsymbol{\sigma}_t\mathrm{i}\frac{K-1}{4c}|\chi_\nu\gamma'\rangle + \\ & \langle\chi_\mu\gamma|\mathrm{i}\frac{K-1}{4c}\boldsymbol{\sigma}\mathbf{r}_\mu\cdot p_t + p_t\boldsymbol{\sigma}\cdot\mathbf{r}_\nu i\frac{K-1}{4c}|\chi_\nu\gamma'\rangle + aK_{\mu\nu,t}^{\gamma\gamma',(1)} \end{aligned} \tag{9}$$

In eq 9, the scalar factor K, which is defined by

$$K = [1 - V/2c^2]^{-1} \tag{10}$$

should not be confused with the matrix elements of the perturbed exchange operator

$$\begin{aligned} K_{\mu\nu,t}^{\gamma\gamma',(1)} = -\sum_j^{\mathrm{occ}}\sum_{\lambda,\sigma}[& (\mu\sigma|\lambda\nu)_t^{(1)} d_{\lambda j}^{\gamma *} d_{\sigma j}^{\gamma'} + \\ & (\mu\sigma|\lambda\nu)(d_{\lambda j}^{\gamma *} d_{\sigma j,t}^{\gamma',(1)} + d_{\lambda j,t}^{\gamma,(1)*} d_{\sigma j}^{\gamma'})] \end{aligned} \tag{11}$$

where

$$(\mu\sigma|\lambda\nu) = \int\int \chi_\mu^*(1)\chi_\sigma(1)\frac{1}{r_{12}}\chi_\lambda^*(2)\chi_\nu(2)\mathrm{d}\tau_1\mathrm{d}\tau_2 \tag{12}$$

$$\begin{aligned} (\mu\sigma|\lambda\nu)_t^{(1)} = {} & \frac{\mathrm{i}}{2c}\int\int \chi_\mu^*(1)\chi_\sigma(1)\frac{1}{r_{12}}\chi_\lambda^*(2)\chi_\nu(2)\times \\ & (\mathbf{R}_{\mu\sigma}\times\mathbf{r}_1 + \mathbf{R}_{\lambda\nu}\times\mathbf{r}_2)_t\mathrm{d}\tau_1\mathrm{d}\tau_2 \end{aligned} \tag{13}$$

$$d_{\lambda j,t}^{\gamma,(1)} = \sum_i^{\mathrm{all}} u_{ji,t}^{(1)} d_{\lambda i}^{\gamma} \tag{14}$$

In eqs 9 and 13 the vectors $\mathbf{r}_\mu = \mathbf{r} - \mathbf{R}_\mu$ and $\mathbf{R}_{\mu\nu} = \mathbf{R}_\mu - \mathbf{R}_\nu$ are introduced from the GIAO derivatives.[2,3]

It should be noted here that when spin−orbital coupling is present, it yields nonzero first-order change in the perturbed density. However, it is usually very small and was neglected in the previous ZORA nonhybrid implementation of the NMR shielding tensor.[2] We have employed here a similar approximation. In addition to spin−orbital coupling, we also have contribution from the nonlocal Hartree−Fock exchange operator. It yields nonzero first-order change in the perturbed density matrix, which cannot be neglected. We have taken this into account through a solution of the coupled-perturbed Hartree−Fock equations as described in ref 3.

The essence of our implementation consists of the approximation of the two-electron integrals with STOs, $(\mu\sigma|\lambda\nu)$ and $(\mu\sigma\mathrm{r}|\lambda\nu)$, by a double fitting formula[4]

$$(\mu\sigma|\lambda\nu) = \sum_{ij} c_i^{\mu\sigma}(f_i|f_j)c_j^{\lambda\nu} \tag{15}$$

$$(\mu\sigma\mathbf{r}|\lambda\nu) = \sum_{ij} c_i^{\mu\sigma}(f_i\mathbf{r}|f_j)c_j^{\lambda\nu} \quad (16)$$

In eqs 15 and 16, the f_i's are the Slater-type fit functions and the $c_i^{\mu\sigma}$'s are the corresponding fit coefficients, obtained from the minimization of the quadratic form[20]

$$\Omega_{\mu\nu} = (\mu\nu - \sum_i c_i^{\mu\nu} f_i|\mu\nu - \sum_i c_i^{\mu\nu} f_i) \quad (17)$$

Despite the approximations made in eqs 15 and 16, in our previous work,[4] we have obtained nonrelativistic NMR shielding constants that are very similar to those calculated by Watson et al.[21] The authors of ref 21 have used a more accurate formula for the calculation of the exchange integrals over STOs. Their scheme includes numerical evaluation of the three-center two-electron integrals with STOs and, due to the higher computational cost, affords hybrid DFT calculations with relatively small molecules only. Our computational scheme allows us to perform STO-based calculations on large transition-metal complexes with inclusion of relativistic effects.

3. Computational Details

We have implemented the algorithm for solving the coupled perturbed Hartree−Fock equations with spin−orbital coupling and GIAOs in the ADF package.[22] The ZORA Hamiltonian with spin−orbital coupling and the polarized valence triple-ζ (TZP) or the double-polarized valence triple-ζ (TZ2P) basis sets from the standard ADF library have been employed for the calculation of the NMR chemical shifts. In this work, we have used B3LYP,[23−25] BP86,[26−28] and BLYP[24,26] functionals as well as the Hartree−Fock method. The geometries for the Hf, Ta, W, Re, Os, Ir, and Hg carbonyls were taken from Wolff and Ziegler,[8] and the structures of a series of Pt(II) complexes were taken from Gilbert and Ziegler.[9] The geometries of the osmium complexes have been optimized at the BP86/DZP/ZORA level of theory with spin−orbital coupling in the Hamiltonian. The structures for hydrogen halides were taken from ref 3.

TABLE 1: ^{1}H NMR Chemical Shifts (ppm) Relative to the HF Molecule[a]

molecule	B3LYP	BP86	Hartree−Fock	others[b]	expt[c]
HCl	−1.96	−1.65	−2.28	−2.57	−2.58
HBr	−4.91	−4.23	−6.80	−4.86	−6.43
HI	−12.58	−10.8	−19.7	−13.49	−15.34

[a] Conditions: integration 5.0; TZ2P basis set; GIAOs; ZORA spin−orbital coupling. [b] Hartree−Fock ZORA with spin−orbital coupling results from ref 3. [c] Experimental values are taken from ref 8.

4. Results of Calculations and Discussion

In Table 1, we have listed the calculated and experimental ^{1}H NMR chemical shifts in hydrogen halides. For comparison, we have also given the results of calculations from ref 3. According to the table, the DFT results are underestimated, and the Hartree−Fock results for HBr and HI are overestimated in absolute value. Our Hartree−Fock NMR shifts are lower than those from the work of Fukui and Baba[3] for HBr and HI but a bit higher for HCl. Because we have used the same level of approximation, the source of deviation is in the basis set. Fukui's proton shift for the HCl molecule (see Table 1) is almost identical to that of experiment, while our Hartree−Fock proton shift for the HBr molecule is much closer to that of experiment. The largest deviation that we have found for the Hartree−Fock proton shifts is for the HI molecule. Our result is lower by approximately 45% than that from ref 3 and is almost twice as large as the proton shift from the BP86 functional.

Results from the calculation of ^{13}C NMR chemical shifts in metal carbonyls are compared to experimental values in Table 2. We have also listed in the same table absolute deviations from experiment expressed in percents. Tetramethylsilane (TMS) was used as the NMR reference sample. The TMS shielding constants in ppm are 180.34, 175.90, 180.06, and 190.94 for BP86, BLYP, B3LYP, and Hartree−Fock, respectively. As we can see from Table 2, the largest deviation from experiment is obtained in the case of the BP86 and BLYP functionals for the chemical shifts in the $Hf(CO)_6^{2-}$ and $Hg(CO)_2^{2+}$ complexes. For the Hartree−Fock method, we have obtained the opposite trend, namely, the smallest deviation from experiment is for the Hf and Hg carbonyl complexes. The chemical shifts from the BLYP functional are underestimated with respect to experiment for the Hf and Hg carbonyls and overestimated for other systems. The chemical shifts from the Hartree−Fock method are all overestimated, with the exception of those for $Ir(CO)_6^{3+}$. The chemical shifts produced by the B3LYP functional are in between the corresponding values from the BLYP functional and the Hartree−Fock method, which is in agreement with the fact that B3LYP contains 20% of the exact Hartree−Fock exchange. Therefore, it is not a surprise that the chemical shifts produced by the B3LYP functional agree better with those from experiment for the Hf and Hg carbonyls than those from BLYP. For other carbonyls, the increase of the calculated NMR chemical shifts leads to larger deviations from the experimental values.

In Table 3, we have listed for the same set of carbonyls as those in Table 2 the HOMO−LUMO gaps as well as the diamagnetic, paramagnetic, and spin−orbit contributions to the total calculated chemical shifts for the BLYP functional and Hartree−Fock method. First of all, in the row from Hf to Ir, the spin−orbit contribution increases. Such a trend was also

TABLE 2: ^{13}C NMR Chemical Shifts (ppm) Relative to the TMS molecule[a]

	BP86		BLYP		B3LYP		Hartree−Fock		
molecule	δ	dev.(%)	δ	dev.(%)	δ	dev.(%)	δ	dev.(%)	expt[b]
$Hf(CO)_6^{2-}$	231.79	5.00	237.17	5.79	244.57	0.23	263.34	7.93	244
$Ta(CO)_6^{1-}$	210.19	0.38	213.20	1.04	221.39	4.92	242.50	14.93	211
$W(CO)_6$	192.25	0.13	194.05	1.07	202.63	5.35	223.37	16.34	192
$Re(CO)_6^{1+}$	173.41	1.41	174.57	2.09	182.49	6.72	197.70	15.61	171
$Os(CO)_6^{2+}$	150.62	2.46	151.61	3.14	157.44	7.10	160.11	8.92	147
$Ir(CO)_6^{3+}$	125.97	4.11	126.82	4.81	129.61	7.12	108.33	10.47	121
$Hg(CO)_2^{2+}$	155.20	8.06	150.26	10.98	158.24	6.25	179.01	6.05	168.8
rmsd	7.35		8.17		9.62		22.36		

[a] Conditions: TZP basis set; GIAOs; ZORA spin−orbital coupling. [b] Experimental values are taken from ref 8.

TABLE 3: Diamagnetic, Paramagnetic, and Spin−Orbit Contributions to ^{13}C NMR Chemical Shifts (ppm) Relative to the TMS Molecule and the HOMO−LUMO Gaps (eV)[a]

	BLYP				Hartree−Fock			
molecule	Δ_{HL}	δ_D	δ_P	δ_{SO}	Δ_{HL}	δ_D	δ_P	δ_{SO}
$Hf(CO)_6^{2-}$	1.87	−23.80	260.72	−0.247	6.88	−34.29	298.56	0.933
$Ta(CO)_6^{1-}$	2.55	−27.19	243.86	3.466	8.41	−37.91	286.99	6.572
$W(CO)_6$	3.34	−29.73	232.07	8.297	10.17	−39.90	278.47	15.208
$Re(CO)_6^{1+}$	4.14	−30.75	221.19	15.871	12.10	−40.65	268.15	29.794
$Os(CO)_6^{2+}$	5.21	−31.39	207.30	24.301	14.58	−41.40	250.65	49.139
$Ir(CO)_6^{3+}$	5.90	−31.33	190.71	32.562	16.89	−41.49	229.03	79.217
$Hg(CO)_2^{2+}$	7.25	−28.82	167.12	−11.959	17.35	−39.42	200.39	−18.037

[a] Conditions: TZP basis set; GIAOs; ZORA spin−orbital coupling.

TABLE 4: ^{195}Pt NMR Chemical Shifts (ppm) Relative to the *cis*-$PtCl_2(SMe_2)_2$ Molecule and Spin−Orbit Contributions to the Total Calculated Shifts[a]

	BP86		B3LYP		BLYP		
molecule	δ_{SO}	δ	δ_{SO}	δ	δ_{SO}	δ	expt[b]
cis-$PtCl_2(SMe_2)_2$	0	0	0	0	0	0	0
trans-$PtCl_2(SMe_2)_2$	−327.44	614.69	−296.54	759.43	−335.11	633.68	127
cis-$PtBr_2(SMe_2)_2$	−137.42	−352.37	−123.73	−388.43	−135.45	−360.53	−328
trans-$PtBr_2(SMe_2)_2$	−520.34	16.46	−469.59	129.66	−528.92	19.43	−348
cis-$PtI_2(SMe_2)_2$	−366.40	−932.71	−333.62	−1048.66	−353.93	−949.69	
trans-$PtI_2(SMe_2)_2$	−936.02	−1112.86	−857.42	−1068.06	−946.71	−1147.18	−1601
cis-$PtCl_2(NH_3)_2$	−315.65	1283.67	−313.58	1535.80	−333.52	1420.04	1447
trans-$PtCl_2(NH_3)_2$	−231.40	1202.55	−221.67	1526.35	−246.35	1288.62	1450
cis-$PtBr_2(NH_3)_2$	−463.42	802.49	−444.30	1031.40	−476.10	925.86	1092
trans-$PtBr_2(NH_3)_2$	−358.85	676.61	−315.48	1000.85	−367.00	753.08	
cis-$PtI_2(NH_3)_2$	−746.60	−137.24	−692.77	20.52	−735.94	−44.88	283
trans-$PtI_2(NH_3)_2$	−664.75	−313.71	−583.66	−27.21	−659.60	−266.05	
cis-$PtCl_2(PMe_3)_2$	51.48	−362.23	93.01	−598.17	63.51	−383.29	−857
trans-$PtCl_2(PMe_3)_2$	10.29	−202.89	−6.17	−297.14	19.87	−187.51	−399
cis-$PtBr_2(PMe_3)_2$	−63.06	−582.34	−28.29	−869.12	−62.37	−618.92	−1085
trans-$PtBr_2(PMe_3)_2$	−159.73	−749.74	−129.43	−837.28	−153.99	−743.89	−922
cis-$PtI_2(PMe_3)_2$	−231.33	−911.75	−203.89	−1256.27	−247.28	−975.03	−1037
trans-$PtI_2(PMe_3)_2$	−474.71	−1700.15	−389.72	−1816.40	−479.42	−1729.96	−1988
cis-$PtCl_2(AsMe_3)_2$	−66.52	−392.22	−18.19	−554.92	−57.86	−404.70	−740
trans-$PtCl_2(AsMe_3)_2$	−58.74	−120.31	−59.50	−131.54	−50.53	−93.47	−229
cis-$PtBr_2(AsMe_3)_2$	−208.87	−686.61	−150.98	−878.56	−204.02	−709.01	−1074
trans-$PtBr_2(AsMe_3)_2$	−227.33	−684.68	−191.19	−705.10	−223.03	−666.0	−827
cis-$PtI_2(AsMe_3)_2$	−442.50	−1166.58	−385.63	−1421.74	−447.96	−1214.17	
trans-$PtI_2(AsMe_3)_2$	−543.18	−1721.28	−462.58	−1795.25	−548.49	−1736.59	−1967
rmsd		323		265		298	

[a] Conditions: TZP basis set; GIAOs; ZORA spin−orbital coupling. [b] Experimental values are taken from ref 9.

observed in ref 8. Nevertheless, the largest contribution to the NMR chemical shift is from the paramagnetic part of the shielding tensor. We can also see that the Hartree−Fock method yields larger HOMO−LUMO gaps (see Table 3) and larger paramagnetic chemical shifts than the BLYP functional. In order to explain this effect, we need to consider the matrix elements of the *u* matrices (see eq 5), which contribute to the paramagnetic term of the shielding tensor through the perturbed orbitals. An increase of the orbital energy differences which constitute the denominator of *u* reduces an overall contribution to the paramagnetic tensor. On the other hand, a simultaneous increase of the numerator of eq 5, which includes the magnetic coupling of the occupied and virtual orbitals, might lead to an overall increase of the paramagnetic NMR tensor. The last situation is true for the Hartree−Fock method; the effect of an increase of the numerator outperforms the effect of an increase of the denominator. This result corroborates findings of the authors of refs 29 and 30. However, in the row from Hf to Hg, an increase of the HOMO−LUMO gap leads to a decrease of the paramagnetic part of the chemical shift for both methods.

The results of statistical averaging shows that the B3LYP functional does not improve the agreement with experiment, but its performance is not much worse than the performance of BLYP or BP86. Thus, the root-mean-square deviation (rmsd) with respect to experiment for B3LYP is 9.62 compared to 8.17 for BLYP and 7.35 for BP86. However, the Hartree−Fock method performs much worse. Its rmsd is 22.36, which is approximately twice as large as the B3LYP value.

In Table 4, we have listed the calculated and experimental ^{195}Pt NMR chemical shifts together with spin−orbit contributions to the total calculated chemical shifts. The *cis*-$PtCl_2(SMe_2)_2$ molecule was used as the NMR reference sample. Its shielding constants in ppm are 6401.0, 6157.4, and 6306.9 for BP86, BLYP, and B3LYP, respectively. The results of calculations with the pure functionals as well as B3LYP are in a good agreement with experimental trends. For example, the ^{195}Pt chemical shifts of PtX_2L_2 (where X is Cl, Br, or I) become more negative in the row from Cl to I for each L (where L is SMe_2, NH_3, PMe_3, or $AsMe_3$). Also, the chemical shifts of the $PtX_2(NH_3)_2$ compounds are more positive than those for $PtX_2(PMe_3)_2$ or $PtX_2(AsMe_3)_2$. These trends were also obtained for the calculated Pt^{195} NMR chemical shifts in ref 9. The authors of that work had performed calculations for Pt(II) square-planar complexes with the Pauli and ZORA spin−orbit Hamiltonians, based on the PW91 functional and the frozen core approximation. It was shown in ref 9 that the trend toward more negative shift from Cl toward I is due to spin−orbital coupling. This explanation is also born out of the present set of

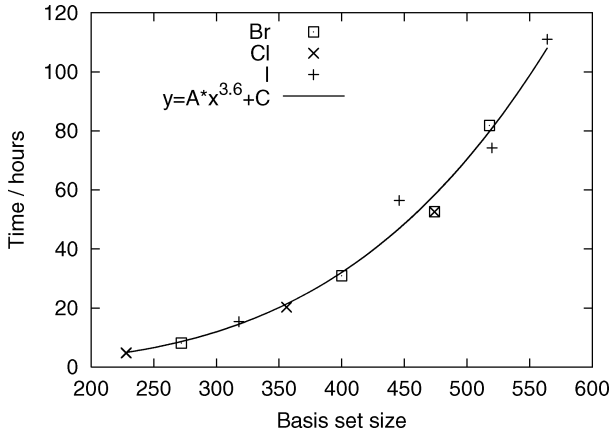

Figure 1. Time scaling of the hybrid NMR calculations on one 2.4 GHz AMD processor for *trans*-PtX_2Y_2 complexes (X = Cl, Br, I); TZP basis set; B3LYP functional; integration 5.0.

TABLE 5: ^{187}Os NMR Chemical Shifts (ppm) Relative to the OsO_4 molecule and the HOMO−LUMO Gaps (eV)[a]

	BP86		B3LYP		BLYP		
molecule	Δ_{HL}	δ	Δ_{HL}	δ	Δ_{HL}	δ	expt.[b]
$OsCpH(PMe_3)_2$	3.414	−5453	4.256	−5383	3.109	−5359	−5272
$OsCpCH_3(PMe_3)_2$	3.315	−4879	4.217	−4736	2.973	−4758	−4779
$OsCpBr(PMe_3)_2$	2.610	−3647	4.197	−3242	2.583	−3518	−3506

[a] Conditions: TZP basis set; GIAOs; ZORA spin−orbital coupling. [b] The experimental values are taken from ref 32.

calculations; see Table 4. The trend with respect to the ligand L has been explained previously,[9] and the analysis will not be repeated here. It was also shown in ref 31 that such spin−orbit effects originate both from the Pt atom and from the ligands.

The largest deviation between the BP86, BLYP results and experiment is found for *trans*-$PtCl_2(SMe_2)_2$ and its iodide homologue and also for *cis*-$PtCl_2(PMe_3)_2$ and its bromide homologue. As for the B3LYP results, the largest deviation is found for the *trans*-$PtCl_2(SMe_2)_2$ molecule and its bromide and iodide homologues. It can be seen from Table 4 that, in most cases, the B3LYP functional yields better agreement with experiment than BP86 and BLYP. For the *cis*-$PtI_2(NH_3)_2$ molecule, B3LYP predicts the correct sign, while BP86 and BLYP do not. The platinum chemical shifts are better described by the nonhybrid functionals for the $PtX_2(SMe_2)_2$ compounds. Comparison of the rmsd value of B3LYP (265) against the BLYP value (298) and the BP86 value (323) shows that, on average, the B3LYP chemical shifts agree better with experiment. As was shown in ref 13, inclusion of the solvation effects into the computational scheme might improve the agreement with experiment, but this is beyond the scope of this paper.

In order to estimate the computational cost of the implemented algorithm and its scaling with the problem size, we have studied the dependence of the total CPU time required for the hybrid NMR calculations versus the basis set size. Figure 1 shows the timings in hours for the hybrid NMR calculations for *trans*-PtX_2Y_2 complexes from Table 4. The basis set size is given in a number of the basis set functions. It can be seen (see Figure 1) that the computational time scales according to a power law with the exponent 3.6. Such a slow performance is caused by the fact that we have implemented at this stage the computation of the GIAO integrals numerically.

In Table 5, we have listed the calculated and experimental ^{187}Os NMR chemical shifts together with HOMO−LUMO gaps. The OsO_4 molecule was used as the NMR reference sample. The B3LYP chemical shifts agree better with experiment than the BP86 values for the $OsCpH(PMe_3)_2$ and $OsCpCH_3(PMe_3)_2$ molecules. The BLYP functional outperforms B3LYP for $OsCpCH_3(PMe_3)_2$ and $OsCpBr(PMe_3)_2$. For the $OsCpH(PMe_3)_2$ molecule, both the BLYP and B3LYP functionals yield the deviation from experiment of approximately the same magnitude but with an opposite sign. It is interesting to note that, although the B3LYP HOMO−LUMO gaps are larger than the corresponding BLYP values for all three molecules, the increase of the gap affects the chemical shifts of three molecules in a different way. For $OsCpH(PMe_3)_2$, an increase of the HOMO−LUMO gap by approximately 1.15 eV leads to a small increase (24 ppm in absolute value) of the B3LYP chemical shift. For $OsCpCH_3(PMe_3)_2$, an increase of the HOMO−LUMO gap by approximately 1.2 eV leads to a small decrease (22 ppm in absolute value) of the B3LYP chemical shift. For $OsCpBr(PMe_3)_2$, an increase of the HOMO−LUMO gap by approximately 1.6 eV leads to a substantial decrease (276 ppm in absolute value) of the B3LYP chemical shift.

In order to clarify this situation, we have decomposed the total calculated NMR chemical shifts into the diamagnetic, paramagnetic, and spin−orbit parts and listed them in Table 6. It can be seen, first of all, that the diamagnetic contribution to the total chemical shift is negligible. Second, the changes in the spin−orbit and paramagnetic parts for the $OsCpH(PMe_3)_2$ and $OsCpCH_3(PMe_3)_2$ molecules compensate each other when the B3LYP and BLYP values are compared. However, for the $OsCpBr(PMe_3)_2$ molecule, both the spin−orbit and paramagnetic parts increase from BLYP to B3LYP.

5. Summary

In this work, we have presented the implementation of the fast and accurate algorithm for the calculation of the NMR shielding tensor with STOs and the ZORA Hamiltonian with spin−orbital coupling. It is based on a double fitting formula for the Hartree−Fock exchange integrals. We have tested this method on 5d transition-metal complexes. In most cases, the B3LYP functional yields larger chemical shifts (in absolute value) than BLYP. As a result, the application of the B3LYP functional yields smaller deviations from experiment for the ^{195}Pt NMR chemical shifts in comparison to BLYP values. It happens because for the majority of studied Pt(II) square complexes, local functionals (BLYP and BP86) underestimate (in absolute value) the NMR chemical shifts.

In osmium complexes, the situation is different. The BLYP functional yields ^{187}Os chemical shifts that are very close to

TABLE 6: Diamagnetic, Paramagnetic, and Spin−Orbit Contribution to ^{187}Os NMR Chemical Shifts (ppm)[a]

	BP86			B3LYP			BLYP		
molecule	δ_D	δ_P	δ_{SO}	δ_D	δ_P	δ_{SO}	δ_D	δ_P	δ_{SO}
$OsCpH(PMe_3)_2$	−7	−5271	−175	−10	−5296	−76	−7	−5180	−174
$OsCpCH_3(PMe_3)_2$	−8	−4691	−179	−12	−4644	−79	−8	−4572	−179
$OsCpBr(PMe_3)_2$	−9	−3369	−270	−11	−3056	−174	−9	−3243	−268

[a] Conditions: TZP basis set; GIAOs; ZORA spin−orbital coupling.

experimental values. Therefore, the B3LYP functional either does not improve calculated NMR shifts or increases the deviation from experiment. The B3LYP functional also outperforms BP86 for two osmium complexes.

For the ^{13}C NMR chemical shifts in 5d metal carbonyls, we have not found improvements from the application of the B3LYP functional for the majority of studied systems.

Acknowledgment. One of the authors, T.Z., thanks the Canadian Government for a Canada Research Chair.

References and Notes

(1) Pyykkö, P. Theory of NMR parameters. From Ramsey to relativity, 1953 to 1983. In *Calculation of NMR and EPR Parameters. Theory and Applications*; Kaupp, M., Bühl, M., Malkin, V. G., Eds.; Wiley-VCH: Weinheim, Germany, 2004.

(2) Wolff, S. K.; Ziegler, T.; van Lenthe, E.; Baerends, E. J. *J. Chem. Phys.* **1999**, *110*, 7689–7698.

(3) Fukui, H.; Baba, T. *J. Chem. Phys.* **2002**, *117*, 7836–7844.

(4) Krykunov, M.; Ziegler, T.; van Lenthe, E. *Int. J. Quantum Chem.* **2009**, *109*, 1676–1683.

(5) Autschbach, J. *J. Chem. Phys.* **2008**, *129*, 094105.

(6) Ye, A.; Patchkovskii, S.; Autschbach, J. *J. Chem. Phys.* **2007**, *127*, 074104.

(7) Krykunov, M.; Ziegler, T. *Int. J. Quantum Chem.* **2009**, *109*, 3246–3258.

(8) Wolff, S. K.; Ziegler, T. *J. Chem. Phys.* **1998**, *109*, 895–905.

(9) Gilbert, T. M.; Ziegler, T. *J. Phys. Chem. A* **1999**, *103*, 7535–7543.

(10) Fowe, E. P.; Belser, P.; Daul, C.; Chermette, H. *Phys. Chem. Chem. Phys.* **2005**, *7*, 1732–1738.

(11) Kramer, J.; Koch, K. *Inorg. Chem.* **2006**, *45*, 7843–7855.

(12) Koch, K. R.; Burger, M. R.; Kramer, J.; Westra, A. N. *Dalton Trans.* **2006**, 3277–3284.

(13) Sterzel, M.; Autschbach, J. *Inorg. Chem.* **2006**, *45*, 3316–3324.

(14) Autschbach, J. *Coord. Chem. Rev.* **2007**, *251*, 1796–1821.

(15) Still, B. M.; Anil Kumar, P. G.; Aldrich-Wright, J. R.; Price, W. S. *Chem. Soc. Rev.* **2007**, *36*, 665–686.

(16) Bühl, M. *Annu. Rep. NMR Spectrosc.* **2008**, *64*, 77–126.

(17) Hada, M.; Ishikawa, Y.; Nakatani, J.; Nakatsuji, H. *Chem. Phys. Lett.* **1999**, *310*, 342–346.

(18) Visscher, L.; Enevoldsen, T.; Saue, T.; Jensen, H. J. A.; Oddershede, J. *J. Comput. Chem.* **1999**, *20*, 1262–1273.

(19) van Leeuwen, R.; van Lenthe, E.; Baerends, E. J.; Snijders, J. G. *J. Chem. Phys.* **1994**, *101*, 1272.

(20) Watson, M. A.; Handy, N. C.; Cohen, A. J. *J. Chem. Phys.* **2003**, *119*, 6475–6481.

(21) Watson, M. A.; Handy, N. C.; Cohen, A. J.; Helgaker, T. *J. Chem. Phys.* **2004**, *120*, 7252–7261.

(22) Baerends, E. J.; Autschbach, J.; Berger, J. A.; Bérces, A.; Bickelhaupt, F. M.; Bo, C.; de Boeij, P. L.; Boerrigter, P. M.; Cavallo, L.; Chong, D. P.; Deng, L.; Dickson, R. M.; Ellis, D. E.; van Faassen, M.; Fan, L.; Fischer, T. H.; Fonseca Guerra, C.; van Gisbergen, S. J. A.; Götz, A. W.; Groeneveld, J. A.; Gritsenko, O. V.; Grüning, M.; Harris, F. E.; van den Hoek, P.; Jacob, C. R.; Jacobsen, H.; Jensen, L.; Kadantsev, E. S.; van Kessel, G.; Klooster, R.; Kootstra, F.; Krykunov, M. V.; van Lenthe, E.; Louwen, J. N.; McCormack, D. A.; Michalak, A.; Neugebauer, J.; Nicu, V. P.; Osinga, V. P.; Patchkovskii, S.; Philipsen, P. H. T.; Post, D.; Pye, C. C.; Ravenek, W.; Rodriquez, J. I.; Romaniello, P.; Ros, P.; Schipper, P. R. T.; Schreckenbach, G.; Snijders, J. G.; Solá, M.; Swart, M.; Swerhone, D.; te Velde, G.; Vernooijs, P.; Versluis, L.; Visscher, L.; Visser, O.; Wang, F.; Wesolowski, T. A.; van Wezenbeek, E. M.; Wiesenekker, G.; Wolff, S. K.; Woo, T. K.; Yakovlev, A. L.; Ziegler, T. Amsterdam Density Functional, Theoretical Chemistry; Vrije Universiteit: Amsterdam, The Netherlands http://www.scm.com, 2008.

(23) Becke, A. D. *J. Chem. Phys.* **1993**, *98*, 5648–5652.

(24) Lee, C.; Yang, W.; Parr, R. G. *Phys. Rev. B* **1988**, *37*, 785.

(25) Stephens, P. J.; Devlin, F. J.; Chabalowski, C. F.; Frisch, M. J. *J. Phys. Chem.* **1994**, *98*, 11623.

(26) Becke, A. D. *Phys. Rev. A* **1988**, *38*, 3098–3100.

(27) Perdew, J. P. *Phys. Rev. B* **1986**, *33*, 8822–8824.

(28) Perdew, J. P. *Phys. Rev. B* **1986**, *34*, 7406.

(29) Schreckenbach, G. *J. Chem. Phys.* **1999**, *110*, 11936–11949.

(30) Wilson, P. J.; Amos, R. D.; Handy, N. C. *Phys. Chem. Chem. Phys.* **2000**, *2*, 187–194.

(31) Autschbach, J.; Zheng, S. *Magn. Reson. Chem.* **2008**, *46*, S45–S55.

(32) Benn, R.; Brenneke, H.; Joussen, E.; Lehmkuhl, H.; Ortiz, F. L. *Organometallics* **1990**, *9*, 756–761.

JP901991S